AGU PUBLICATIONS

JGR

Journal of Geophysical Research: Atmospheres

RESEARCH ARTICLE

10.1002/2014JD022429

Key Points:
- Hemispheric asymmetries and the seasonality of mean age are explained
- Forcing of the Brewer-Dobson circulation quantified in isentropic coordinates
- Different seasonalities of the deep and shallow branches of the Brewer-Dobson circulation

Correspondence to:
P. Konopka,
p.konopka@fz-juelich.de

Citation:
Konopka, P., F. Ploeger, M. Tao, T. Birner, and M. Riese (2015), Hemispheric asymmetries and seasonality of mean age of air in the lower stratosphere: Deep versus shallow branch of the Brewer-Dobson circulation, *J. Geophys. Res. Atmos.*, *120*, 2053–2066, doi:10.1002/2014JD022429.

Received 12 AUG 2014
Accepted 3 FEB 2015
Accepted article online 11 FEB 2015
Published online 4 MAR 2015

Hemispheric asymmetries and seasonality of mean age of air in the lower stratosphere: Deep versus shallow branch of the Brewer-Dobson circulation

Paul Konopka[1], Felix Ploeger[1], Mengchu Tao[1], Thomas Birner[2], and Martin Riese[1]

[1]Forschungszentrum Jülich (IEK-7: Stratosphere), Germany, [2]Department of Atmospheric Science, Colorado State University, Fort Collins, Colorado, USA

Abstract Based on multiannual simulations with the Chemical Lagrangian Model of the Stratosphere, (CLaMS) driven by ECMWF ERA-Interim reanalysis, we discuss hemispheric asymmetries and the seasonality of the mean age of air (AoA) in the lower stratosphere. First, the planetary wave forcing of the Brewer-Dobson circulation is quantified in terms of Eliassen Palm flux divergence calculated by using the isentropic coordinate θ. While the forcing of the deep branch at $\theta = 1000$ K (around 10 hPa) has a clear maximum in each hemisphere during the respective winter, the shallow branch of the Brewer-Dobson circulation, i.e., between 100 and 70 hPa ($380 < \theta < 420$ K), shows almost opposite seasonality in both hemispheres with a pronounced minimum between June and September in the Southern Hemisphere. Second, we decompose the time-tendency of AoA into the contributions of the residual circulation and of eddy mixing by analyzing the zonally averaged tracer continuity equation. In the tropical lower stratosphere between $\pm 30°$, the air becomes younger during boreal winter and older during boreal summer. During boreal winter, the decrease of AoA due to tropical upwelling outweighs aging by isentropic mixing. In contrast, weaker isentropic mixing outweighs an even weaker upwelling in boreal summer and fall making the air older during these seasons. Poleward of 60°, the deep branch locally increases AoA and eddy mixing locally decreases AoA with the strongest net decrease during spring. Eddy mixing in the Northern Hemisphere outweighs that in the Southern Hemisphere throughout the year.

1. Introduction

The annual cycle of the composition of air in the upper troposphere lower stratosphere (UTLS) region is determined by the seasonality of different transport processes like convection, Brewer-Dobson (BD) circulation, and two-way irreversible isentropic transport [*Holton et al.*, 1995; *Fueglistaler et al.*, 2009a; *Gettelman et al.*, 2011]. Significant hemispheric differences of all these transport processes result from the hemispheric asymmetry of the land-sea distribution and of the orography.

The composition of air entering the stratosphere is mainly determined by the transport processes within the tropical tropopause layer (TTL) coupling the Hadley circulation (time scale of days) in the tropical troposphere with the much slower (time scale of months) BD circulation in the stratosphere [*Fueglistaler et al.*, 2009a]. Complementary to the upward transport through the TTL, the downwelling branch of the BD circulation influences the composition in the extratropical stratosphere down to the Extratropical Upper Troposphere Lower Stratosphere (ExUTLS) [*Gettelman et al.*, 2011]. The BD circulation is mechanically driven by planetary wave-induced friction torque that is proportional to the convergence of the Eliassen Palm (EP) flux [*Haynes et al.*, 1991]. This mechanism is often referred to as the extratropical pump [*Holton et al.*, 1995].

Because most of these waves are generated in the orography-dominated troposphere, this mechanistic picture is usually referred to as the "tropospheric control" of the BD circulation [*Rosenlof*, 1995; *Gerber*, 2012]. As introduced by *Plumb* [2002] and discussed by *Birner and Bönisch* [2011], one should distinguish two separate branches of the BD circulation itself: a shallow branch, between 100 and 70 hPa, transporting air into the extratropics [*Rosenlof*, 1995], and a deep branch between 70 and 1 hPa, with a maximum around 10 hPa, driven by planetary and gravity waves reaching into the upper stratosphere and mesosphere.

On the other hand, the theoretical work of *Charney and Drazin* [1961] suggests that easterly summer winds and sufficiently strong westerlies limit Rossby wave propagation into the stratosphere, thus reducing the BD circulation at higher levels with larger wave activity during winter in the Northern Hemisphere (NH) than in

the Southern Hemisphere (SH) [*Plumb*, 1989]. Based on sensitivity studies with an idealized general circulation model, *Gerber* [2012] suggested that the strength of the stratospheric polar vortex indirectly affects the BD circulation. A colder vortex creates a waveguide higher into the stratosphere, raising the breaking level of Rossby waves and deepening the circulation. *Gerber* [2012] termed this type of influence on the BD circulation as "stratospheric control."

As first envisioned by *Brewer* [1949] and *Dobson* [1956], the BD circulation is fundamentally connected to the transport of chemical species. A commonly used metric of transport is the mean age of air (AoA) defined as the first moment of the age spectrum [*Hall and Plumb*, 1994; *Waugh and Hall*, 2002]. As each air parcel is a mixture of particles with different transit times since their last contact with the Earth's surface, the age spectrum itself can be understood as a distribution of such transit times and AoA as a mean transit time averaged over this ensemble. AoA can be estimated from observations [*Andrews et al.*, 2001; *Waugh and Hall*, 2002; *Stiller et al.*, 2008] and is a convenient diagnostic to visualize the variability and trends in the distribution of transport paths [*Austin and Li*, 2006; *Garcia and Randel*, 2008; *Butchart et al.*, 2010; *Diallo et al.*, 2012; *Li et al.*, 2012].

The main goal of this paper is to understand the hemispheric differences and the seasonality of AoA in the lower stratosphere, especially in the vicinity of the tropopause. Therefore, we proceed in two steps: In the first step we analyze the forcing of the BD circulation by using the isentropic EP flux diagnostics based on the European Centre for Medium-range Weather Forecasts (ECMWF) meteorological ERA-Interim reanalysis [*Dee et al.*, 2011]. This reanalysis represents well the BD circulation by reproducing the seasonality of H_2O observed by the Aura Microwave Limb Sounder (MLS) [*Hegglin et al.*, 2014, and references therein] and due to similar upward mass flux at 70 hPa if compared with other reanalyses and climate-chemistry models [*Seviour et al.*, 2012].

In the second step, we analyze the distribution of AoA as caused by the BD circulation. AoA was derived from the Chemical Lagrangian Model of the Stratosphere (CLaMS) [*McKenna et al.*, 2002; *Pommrich et al.*, 2014]. The BD circulation includes net mass transport and two-way mixing [see, e.g., *Bönisch et al.*, 2011]. The mass transport can be described in terms of the 2-D residual circulation either in pressure (TEM formalism) or isentropic coordinates [*Andrews et al.*, 1987]. On the other hand, the bidirectional, horizontal, almost isentropic mixing does not influence the transport of mass but significantly affects the distribution of tracers (like AoA being here a surrogate for the measurable tracers). Here, we use the zonally averaged AoA continuity equation in isentropic coordinates [*Andrews et al.*, 1987] to decompose the time-tendency of AoA into the local forcing of the residual circulation and of the eddy mixing. *Randel et al.* [1994] applied an analogous decomposition (although in pressure coordinates) to interpret the first satellite-based N_2O observations.

In the present study an 11 year CLaMS climatology of AoA covering the period 2002–2012 as well as respective ERA-Interim climatologies of the EP flux divergence and AoA tendencies are investigated. Variabilities related to the Quasi Biennial Oscillation (QBO) or solar cycle are not discussed here. A general discussion of the AoA variability including decadal changes is presented in *Ploeger et al.* [2015]. In section 2, we describe the CLaMS simulations and the climatology of AoA derived from these calculations. The forcing of transport quantified in terms of the EP flux divergence and diabatic heating rates is discussed in section 3. In section 4, the analysis of the zonal mean continuity equation for AoA is presented. Finally, in sections 5 and 6, we discuss and conclude our main findings.

2. Mean Age Derived From CLaMS

2.1. Model Description

The 25 years run CLaMS simulations of AoA (from 1988 to 2012) extend between the Earth's surface and the mesosphere. The horizontal winds are prescribed by the ECMWF ERA-Interim reanalysis [*Dee et al.*, 2011]. The run is initialized with a MIPAS climatology and an 8 years spin-up period by repeating the year 1988. This spin-up time ensures that the initial distribution is only defined by the model transport and boundary condition. The analysis discussed in this paper is limited to the time period 2002–2012 for which also the SF_6-based MIPAS observations are used for model validation.

To resolve both transport processes in the troposphere influenced by the orography and in the stratosphere where adiabatic horizontal transport dominates, a hybrid coordinate is used [*Mahowald et al.*, 2002]. Therefore, in the stratosphere and in the UTLS, potential temperature θ is employed as the vertical

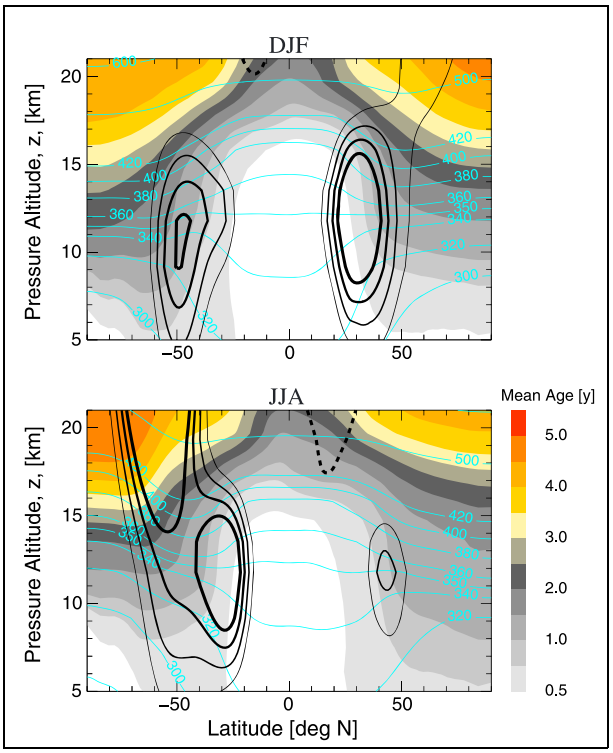

Figure 1. Zonal means of AoA for (top) DJF versus (bottom) JJA as function of the latitude and log-pressure altitude. Black lines are isolines of the zonal wind for 30, 25, 20, and 15 m/s, from thick to thin, respectively (solid lines, westerlies; dashed line, easterlies; cyan lines, isentropes).

coordinate of the model and the cross-isentropic velocity $\dot{\theta} = Q$ is deduced from the ERA-Interim forecast total diabatic heating rates Q, including the effects of all-sky radiative heating, latent heat release, and diffusive heating *Fueglistaler et al.* [2009b], *Ploeger et al.* [2010]. The vertical velocity $\dot{\theta}$ and horizontal winds are available every 6 h.

In the tropospheric region defined by the condition $\sigma = 0.3$, the vertical model coordinate smoothly transforms into an orography-following $\sigma = p/p_s$-coordinate (p, pressure; p_s, surface pressure), with the vertical velocity transforming into the corresponding $\dot{\sigma}$. The specific model setup employed here closely follows the CLaMS configuration described by *Pommrich et al.* [2014] with a vertical and horizontal resolution in the UTLS region of about 400 m and 100 km, respectively.

AoA is determined by considering an artificial tracer that linearly increases in the boundary layer (a so-called "clock tracer"). This orography-following layer has a vertical extension around 1.5 km with the exact value slightly depending on the orography itself. AoA is calculated as the time lag between the tracer value at a given point and the tracer value in the boundary layer [*Hall and Plumb*, 1994; *Waugh and Hall*, 2002; *Schoeberl et al.*, 2005].

The upper boundary is defined by the condition $\theta = 2500$ K (i.e., roughly around the stratopause with $p \approx 0.3$ hPa) and is prescribed by AoA estimated from the Michelson Interferometer for Passive Atmospheric Sounding (MIPAS) observations of SF_6 [*Stiller et al.*, 2008]. The seasonality of AoA derived from MIPAS shows a clear shift by 6 months between the NH and SH. Furthermore, the SH is by almost 2 years older than the NH (not shown).

To exclude the influence of the boundary condition on the hemispheric asymmetry of AoA in the UTLS region discussed here, we repeated our studies by using a symmetrized upper boundary condition, i.e., $f_{sym}(\varphi, t) = 0.5(f(\varphi, t) + f(-\varphi, t))$ with $f(\varphi, t)$ (φ, latitude; t, time) denoting the original, MIPAS-based boundary condition. The results show mostly negligible differences to the reference run below $\theta = 1000$ K with largest difference of the order 1 month at $\theta = 1000$ K (i.e., smaller than 2%). This means that the hemispheric asymmetries, which will be discussed in the following subsection, are much more a result of the explicitly resolved part of the BD circulation in the atmospheric domain used for the simulations reported here.

2.2. Seasonality and Hemispheric Differences of Age of Air

In Figures 1 and 2 we show the 2002–2012 CLaMS climatology of AoA in two different projections: as a zonal mean averaged over the DJF and JJA periods and as a seasonality of the zonal mean averaged in two different vertical slices: north of 60°N and south of 60°S. Figure 1 reflects the main pattern of the BD circulation with young air ascending in the tropics and old air descending in the polar regions.

However, a clear hemispheric asymmetry in AoA can be diagnosed from comparing the top and bottom panels in Figure 1: during the same season, air is always younger in the NH than in the SH. A similar hemispheric asymmetry exists in the zonal wind distributions (black contours). In the winter hemispheres,

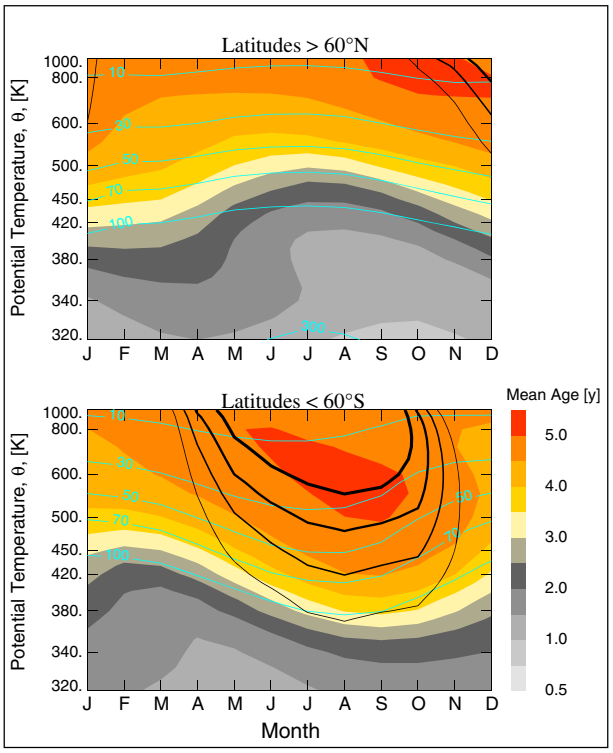

Figure 2. Seasonality of AoA in the (top) northern versus (bottom) southern polar regions shown as zonal means averaged over latitudes north of 60°N and south of 60°S, respectively. The black lines are the isolines of the zonal wind with values of 15, 20, 25, and 30 m/s. The cyan lines describe the isobars. All fields are plotted as a function of (nonequidistant) potential temperature θ. To magnify the UTLS region, the entropy density $s = c_p \rho \ln(\theta/\theta_0)$ with specific heat c_p, air mass density ρ, and the reference potential temperature θ_0 is used as a scaling factor [*Holton et al.*, 1995]. Note that s is maximum around the tropopause. Using this factor, $ds/d\theta$ is kept constant along the vertical axis (for more details, see *Konopka et al.* [2007]).

the subtropical jet forms a strong transport barrier between the tropics and extratropics and the polar jet separates middle and high latitudes in the extratropics. On the other hand, these barriers weaken significantly in the summer hemispheres, most pronounced in the NH [*Haynes and Shuckburgh*, 2000a, 2000b].

Figure 2 shows the vertical structure of the AoA seasonality in high latitudes. In the NH, north of 60°N (Figure 2, top), AoA is always younger than in the SH during the same season (south of 60°S; Figure 2, bottom). The oldest air masses coincide well with the strong zonal winds of the Antarctic polar jet (black). The seasonality is shifted by 6 months between the NH and SH. The youngest extratropical air above the tropopause with $\theta \approx 380$ K can be diagnosed north of 60°N during August and September (and is almost 1 year younger than the youngest air masses south of 60°S during February and March).

A slightly different view on the hemispheric asymmetries of the AoA can be obtained in Figure 3 where the climatologies of AoA are plotted on two isentropes, $\theta = 400$ and 340 K. While isentropic transport on $\theta = 400$ K occurs above the subtropical jet and connects the TTL with high latitudes, the $\theta = 340$ K surface is more characteristic for an isentropic transport pathway below the jet.

Complementary to our previous discussion, the oldest air at $\theta = 400$ K can be found in the SH shortly before the final warming of the Antarctic vortex. Note that signatures of old air within the Antarctic vortex propagate down to $\theta = 340$ K, i.e., to a potential temperature level that can be located in the vicinity of the tropopause. However, to quantify the stratospheric influence in the troposphere, the use of tropopause related coordinates would be more appropriate because of the seasonal cycle and hemispheric differences in location of the isentropes themselves [*Wernli and Sprenger*, 2007].

There is also a clear annual cycle of AoA in the tropics. This can be seen in Figure 3 (top) showing that youngest air at $\theta = 400$ K occurs around February and oldest air occurs around August. At this level, the mean zonal wind almost vanishes in the NH during JJA with the consequence that isentropic two-way mixing transports young air into the high latitudes and old air into the TTL. This distinctive contribution of young tropospheric air to the composition of air in the northern lowermost stratosphere during summer and fall has been derived from the SPURT observations (SPURT - Spurenstofftransport in der Tropopausenregion, trace gas transport in the tropopause region) and was coined as "flushing" of the UTLS region [*Hegglin and Shepherd*, 2007; *Bönisch et al.*, 2009].

The Asian summer anticyclone plays a major role in driving this two-way transport and significantly contributes to the maximum of the seasonal cycle of water vapor in the extratropics and to the maximum in the seasonal cycle of ozone in the TTL [*Konopka et al.*, 2010; *Ploeger et al.*, 2013; *Abalos et al.*, 2013]. The latter transport pathway, i.e., the transport of aged, ozone-rich air from the northern high latitudes into the TTL during JJA has been denoted in-mixing [*Konopka et al.*, 2009].

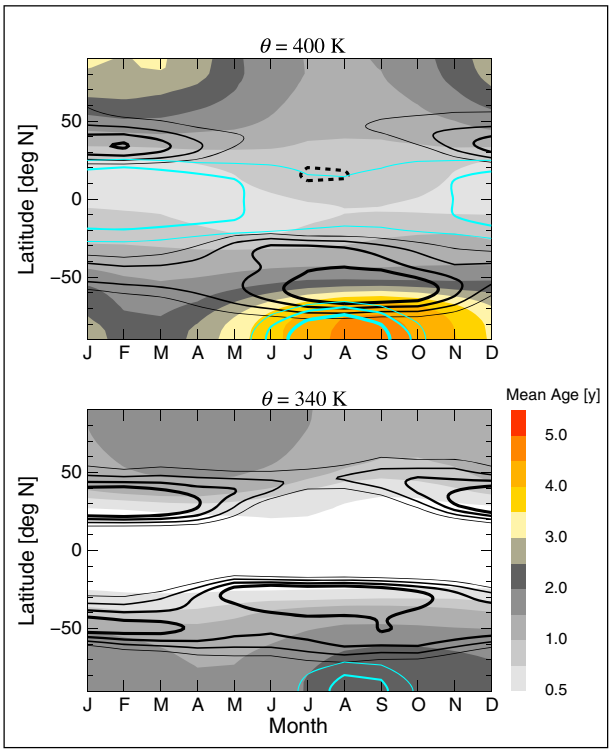

Figure 3. Seasonality of AoA (zonal means) at (top) $\theta = 400$ K and (bottom) 340 K. The black and cyan lines are the isolines of the zonal wind with values of 15, 20, 25, and 30 m/s and temperatures with values of 198, 194, and 190 K from thin to thick, respectively.

2.3. Comparison With the Experimental Data

An important question is how to validate the simulated AoA. As discussed in detail by *Waugh and Hall* [2002], almost all observationally based AoA estimates rely on SF_6 and CO_2 data. Figure 4 shows AoA at 50 hPa (≈19 km) calculated with CLaMS (blue, DJF; red, JJA; vertical extension marks the standard deviation due to year-to-year variability). For comparison, in situ observations discussed by *Waugh and Hall* [2002] are also plotted (black and gray squares for the SF_6 and CO_2-based observations, respectively). In addition, the solid black line depicts the annual mean (and its year-to-year variability) of the recently published, SF_6-based AoA observed from 2002 to 2010 with the MIPAS instrument [*Stiller et al.*, 2012].

Generally, CLaMS AoA underestimates the SF_6-based observations, although the deviation from the CO_2-based data is significantly smaller. The younger simulated mean age in comparison to observations is a typical feature seen in climate models [*Monge-Sanz et al.*, 2007; *SPARC*, 2010]. However, the sparse in situ observations do not sufficiently support the simulated seasonal and hemispheric differences in AoA which are of the order of 1 year.

On the other hand, the simulated asymmetry between the SH and NH can also be seen in the MIPAS observations although the absolute values are around 2 years older than the CLaMS results. *Stiller et al.* [2012] discuss the seasonality of AoA (see Figure 3 in this paper) that has a very similar pattern compared with our studies with oldest air during the austral winter and spring south of 60°S and youngest polar air during the boreal summer and fall north of 60°N, although these features in MIPAS data are more obvious in the altitude range between 22 and 30 km than around 19 km.

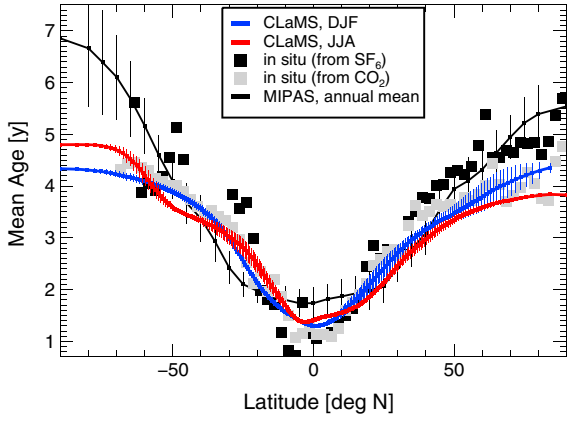

Figure 4. CLaMS simulations versus in situ [*Waugh and Hall*, 2002] and satellite-based MIPAS observations at 50 hPa [*Stiller et al.*, 2012].

3. Wave Forcing of the BD-Circulation Branches

Before analyzing the full transport (i.e., residual circulation and mixing), we discuss now different seasonalities of the shallow and deep branches of the BD circulation and how the different strengths of the Arctic and Antarctic polar vortices modulate this circulation. Following the conventional paradigm of the wave-driven BD circulation, the stratospheric forcing for both residual circulation and eddy mixing is expected to be largely caused by planetary waves. These waves are mainly generated by orography and modulate the zonal mean flow [*Holton et al.*, 1995;

Gerber, 2012]. An established method to quantify the wave forcing is to describe the resolved wave drag in terms of the divergence of the EP flux **F**.

3.1. EP Flux in Isentropic Coordinates

In the isentropic coordinates, the 2-D residual circulation is given by mean meridional and cross-isentropic velocities $(\overline{v}^*, \overline{Q}^*)$ with overbars indicating zonal means weighted with the isentropic mass density σ. We use the same notation as in *Andrews et al.* [1987] (i.e., with stars) although no additional transformation like in the pressure-related TEM formalism is necessary. In the stratosphere, $\overline{Q}^*$ (that is also equal to $\overline{\dot{\theta}}$ introduced in section 2.1) results from the diabatic heating rates which are mainly due to longwave relaxation towards the radiative equilibrium state and due to shortwave absorption. The mean meridional velocity $\overline{v}^*$ fulfills the momentum equation which can be approximated as

$$\partial_t \overline{u} - f\overline{v}^* \sim (\nabla \cdot \mathbf{F})/\overline{\sigma}\,. \tag{1}$$

Here, $\overline{u}$ denotes the zonally averaged zonal wind and f is the Coriolis parameter that is equal 0 at the equator; i.e., equation (1) cannot be used to deduce $\overline{v}^*$ in the deep tropics. Finally, $\nabla \cdot \mathbf{F}$ denotes the divergence of the 2-D EP flux $\mathbf{F} = (F^\varphi, F^\theta)$, which in $(\lambda, \varphi, \theta)$ space (λ, longitude; φ, latitude) is given as [see *Andrews et al.*, 1987, chap. 3.9]:

$$F^\varphi = -a\cos\varphi\,\overline{(\sigma v)'u'}\,,$$
$$F^\theta = g^{-1}\overline{p'M'_\lambda} - a\cos\varphi\,\overline{(\sigma Q)'u'}\,.$$

Here, primes denote the deviations from the zonal means, M is the Montgomery stream function, p pressure, a is the Earth's radius, and g is the acceleration due to gravity.

Thus, resolved waves (here those in the ECMWF ERA-Interim reanalysis) cause a torque decelerating the zonal flow that can be described in terms of the divergence of the EP flux **F**. In a steady state ($\partial_t \overline{u} = 0$), this wave forcing drives the meridional, poleward velocity $\overline{v}^*$ of the BD circulation given by equation (1). The related meridional and poleward heat flow cools the tropics and heats up the high latitudes, shifting the atmosphere out of radiative equilibrium. The relaxation toward the equilibrium state, manifests as $\overline{Q}^*$, i.e., as the cross-isentropic part of the residual circulation. Note that on the seasonal and subseasonal timescale, the steady state picture of the BD circulation may significantly deviate from a more realistic, transient picture with sporadically occurring waves interacting with the mean flow $\overline{u}$ and with all three terms in equation (1) becoming important [*Haynes et al.*, 1991; *Holton et al.*, 1995; *Randel et al.*, 2002].

3.2. Climatology of the EP Flux

In Figure 5, the 2002–2012 climatology of the EP flux divergence divided by $\overline{\sigma}$ is shown (i.e., the right-hand side of equation (1)). In addition, the zonally averaged upwelling due to diabatic heating, i.e., $\overline{Q}^*$, is also depicted (red isolines). In the following, both parameters are used as a proxy for the BD circulation.

While in Figure 5 (top) the total annual mean is plotted, the seasonal and hemispheric differences during the DJF and JJA seasons can be seen in the bottom left and right panels, respectively, of Figure 5. In all three panels, the lower and upper branches of the BD circulation are schematically denoted (thick yellow arrows). As expected, the strength and width of the BD circulation vary with season, with the stronger cell occurring in the winter hemisphere and the upwelling regions shifted toward the summer hemisphere [*Rosenlof*, 1995].

As can be seen in Figure 5 (bottom), the summer easterlies (solid dashed lines) suppress the poleward and upward propagation of the waves with the consequence that the deep branch of the BD circulation disappears during the summer [*Charney and Drazin*, 1961]. Because of the summer easterlies, the meridional boundary of the tropical pipe [*Plumb*, 1996] can be well explained in the respective summer hemisphere above $\theta = 420$ K. In contrast, the tropical pipe boundary in the winter hemisphere manifests solely as a relative minimum of the EP flux divergence separating the shallow from the deep branch of the BD circulation.

The deep branch is stronger during winter in both hemispheres and strongest during northern winter. However, the shallow branch of the BD circulation seems to have a different seasonality. This can be seen by comparing the regions around the subtropical jets below about 500 K, with the EP flux divergence being larger during DJF than during JJA in both hemispheres.

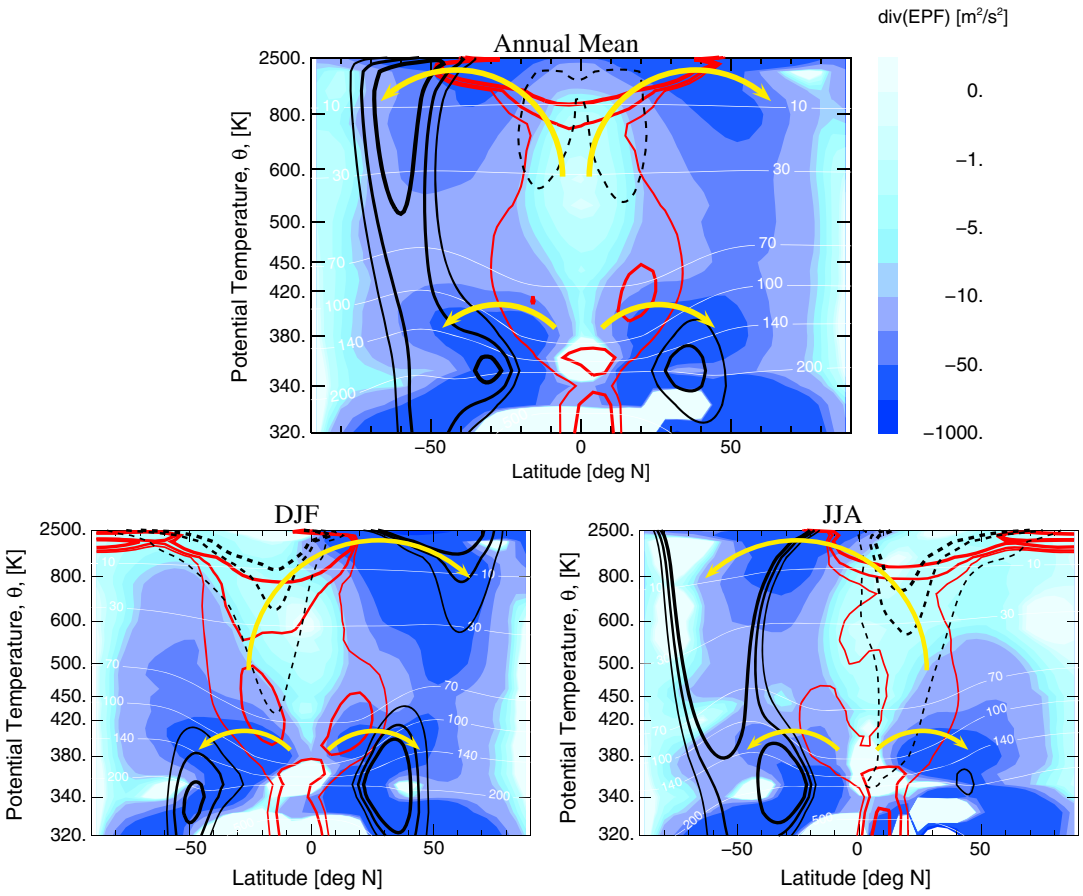

Figure 5. Divergence of the EP flux, as resolved by the ECMWF ERA-Interim winds, which drives the meridional, poleward component of the BD circulation (nonlinear color scale). Nonequidistant potential temperature θ is used as the vertical axis in order to magnify the UTLS region (see caption of Figure 2). The red isolines quantify upwelling due to diabatic heating $\overline{Q}^*$ with values 0.5, 1.0, and 2.0 K/day from thin to thick, respectively. White and black are the isobars and isotachs of the zonal wind, respectively (westerlies: 20, 25, and 30 m/s; easterlies: 10, 20, and 25 m/s from thin to thick). (top) Annual mean. (bottom) DJF (left) versus JJA (right) distribution. The thick yellow arrows schematically denote the shallow (around 400 K or between 100 and 70 hPa) and deep (around 1000 K or 10 hPa) branches of the BD circulation.

To clarify further, Figure 6 shows the annual cycle of the EP flux divergence for two selected θ levels which are exemplarily related to the deep branch (top) and to the shallow branch (bottom) of the BD circulation. The clearest difference between wave forcing at $\theta = 1000$ K and at $\theta = 400$ K is its seasonality. At $\theta = 1000$ K the forcing of the deep branch is shifted by ≈6 month between the NH and SH, with a maximum during winter in the respective hemisphere.

Surprisingly, the shallow branch shows almost opposite seasonality in both hemispheres with a pronounced minimum between June and September in the SH. More precisely, while the deep branch in the SH has its maximum, there is a pronounced minimum in the activity of the SH shallow branch. This minimum of the shallow branch can also be seen in the analysis the effective diffusivity at $\theta = 400$ K [see *Haynes and Shuckburgh*, 2000a, Plate 4]. The maximum of the shallow branch in the NH occurs around May and the minimum around October, i.e., ≈3 month later compared to the NH deep branch.

There is also a clear hemispheric difference in the depth of the poleward penetration of the waves. At $\theta = 1000$ K (Figure 6, top), the dynamical barriers defined by the easterlies and by sufficiently strong westerlies (vortex edges) are obvious. In contrast to the northern high latitudes, the EP flux divergence almost disappears within the southern polar vortex marked by strong zonal winds and low temperatures (this difference can also be deduced by comparing the bottom panels in Figure 5). Thus, the edge of the Antarctic polar vortex blocks effectively the poleward propagation of waves, much more than its counterpart in the NH.

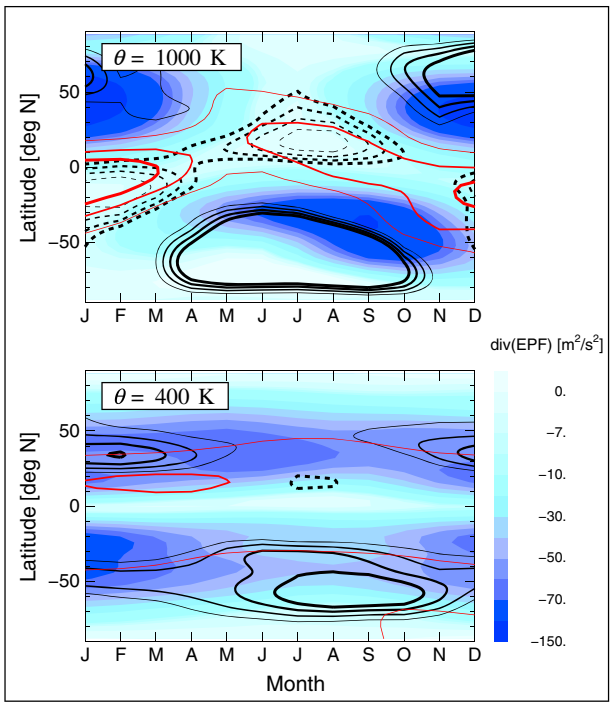

Figure 6. Seasonality of the wave forcing (in terms of the EP flux divergence) at two selected θ levels: (top) 1000 K and (bottom) 400 K. Black solid and dashed lines are westerlies and easterlies, respectively. Red lines denote isolines of $\overline{Q}^* = 1$, 3, 4.5 K/day ($\theta = 1000$ K) and 0, 1.2 K/day ($\theta = 400$ K) from thin to thick, respectively.

It is also worthwhile to note that positive values of the EP flux divergence are generally understood as source regions of the Rossby waves [see, e.g., *Vallis*, 2006]. The regions of positive EP flux divergence (i.e., up-gradient potential vorticity flux) near the subtropical jets (white areas in Figure 5 (bottom)) have recently been discussed by *Birner et al.* [2013].

We summarize that a stronger wave forcing in the NH (see Figure 5, top) favors a stronger residual circulation with shorter transit times connecting the tropical upper troposphere with high latitudes. *Rosenlof* [1995] and more recently *Birner and Bönisch* [2011] have shown (see bottom of their Figure 1) that the transit times into high latitudes (>60°) along the residual circulation are smaller in the NH than in the SH. However, there are strong seasonal differences: During the transition from the winter to summer in the NH, the slow down of the residual circulation is much more pronounced than in the SH (left versus right bottom panel of Figure 5). Furthermore, the hemispheric asymmetries and the seasonal patterns of AoA are not only a result of the residual circulation but also of eddy mixing. Although both processes are driven by waves, the analysis of the EP flux alone does not allow to separate these two transport mechanisms.

4. TEM-Based Analysis of the Mean Age

4.1. Isentropic Decomposition of the AoA Tendencies

A powerful diagnostic tool is to analyze the tracer budget equation for AoA in isentropic coordinates [*Plumb*, 2002; *Ploeger et al.*, 2015]. The zonal mean tracer continuity equation translates into an analogous equation for AoA, in the following denoted with Γ:

$$\partial_t \overline{\Gamma} = 1 + T_{rc} + T_{em} \tag{2}$$

with

$$T_{rc} = -\frac{\overline{v}^*}{a}\partial_\varphi \overline{\Gamma} - \overline{Q}^* \partial_\theta \overline{\Gamma} \tag{3}$$

$$T_{em} = \overline{\sigma}^{-1}[\nabla \cdot \mathbf{M} - \partial_t(\overline{\sigma'\Gamma'})] \approx \overline{\sigma}^{-1} \nabla \cdot \mathbf{M}\,. \tag{4}$$

Here, the terms T_{rc} and T_{em} denote the AoA tendencies due to residual circulation (rc) and due to eddy mixing (em), respectively. T_{em} can be approximated almost everywhere by the divergence of the eddy flux vector $\mathbf{M} = (M^\varphi, M^\theta)$ with $M^\varphi = -\overline{(\sigma v)'\Gamma'}$ and $M^\theta = -\overline{(\sigma Q)'\Gamma'}$. In the tropics and in the high latitudes where the vertical advection dominates (i.e., sufficiently far away from the upward-downward turning points of the BD circulation), T_{rc} can be approximated by the second term in equation (3), i.e., $T_{rc} \approx -\overline{Q}^* \partial_\theta \overline{\Gamma}$ [see *Ploeger et al.*, 2015, Figure 12]. The notation here follows *Andrews et al.* [1987] with overbars indicating mass-weighted zonal means and primes describing the deviations (i.e., fluctuations) from these.

Commonly, T_{rc} and T_{em} are large terms with opposite signs fulfilling the condition (2). It is worthwhile to note that the left and the right-hand sides of (2) are independently calculated and that there is an overall remarkably good agreement between the right- and left-hand sides of equation (2).

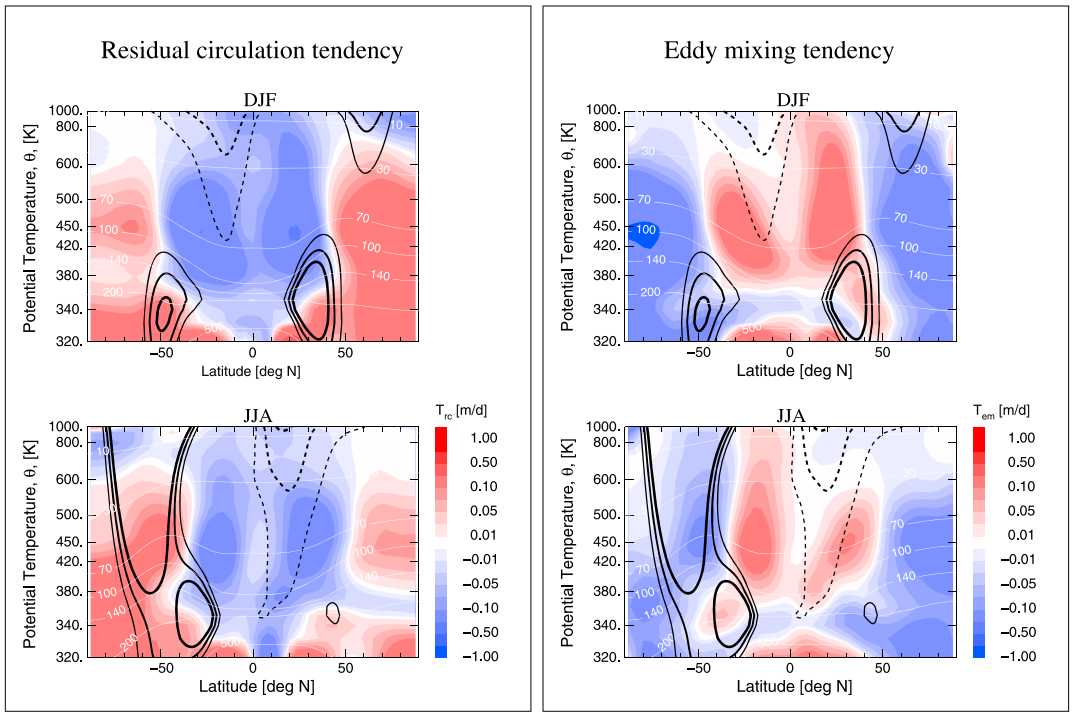

Figure 7. Zonally averaged and mass-weighted (i.e., divided by $\overline{\sigma}$) AoA tendencies due to the residual circulation (T_{rc}, left) and eddy mixing (T_{em}, right) for DJF (top) and JJA (bottom). Nonlinear color scale is used. Zonal winds (black) and isobars (white) are also shown.

4.2. Residual Circulation Versus Eddy Mixing

The decomposition of the total tendency $\partial_t\overline{\Gamma}$ as given by the right-hand side of (2) allows to interpret which type of forcing, advection due to residual circulation or mixing due to eddies, drives the changes of $\overline{\Gamma}$. The DJF and JJA distributions of the mass-weighted tendencies T_{rc} and T_{em} are shown in the left and right columns of Figure 7, respectively.

Generally, the latitudes around $\pm$ 50° separate regions with different properties. Within the tropics and subtropics, AoA is reduced by the upwelling of the residual circulation (blue regions in the left column). Poleward of 50°, AoA increases due to the enhanced downward transport of older air (red regions in the left column). In contrast, eddy mixing increases AoA within the $\pm$50° band and decreases AoA in the high latitudes (red and blue regions in the right column, respectively).

Here we focus on the seasonal and hemispheric differences in this decomposition. Within the $\pm$50° band, the signatures of T_{rc} and T_{em} in both hemispheres are somewhat stronger during DJF than during JJA. In contrast, in the polar regions, strong hemispheric differences can be diagnosed during the same season. For example, absolute values of T_{em} and T_{rc} in the winter high latitudes are larger in the Arctic than in the Antarctic.

Moreover, the downwelling in the NH during DJF causes larger values of T_{rc} if compared with the SH 6 month later, i.e., during JJA. This difference is even stronger in values of T_{em}, with a larger contribution of eddies disturbing the Arctic vortex during DJF relative to the eddy mixing intensity during JJA in the Antarctic.

To see the AoA differences between the tropics and middle and high latitudes more clearly, we average in Figure 8 the mass-weighted tendencies T_{rc} and T_{em} over the vertical range between θ = 380 and 450 K and over three latitude intervals: (a) from 30°S to 30°N for the tropics, (b) between 50–30°S and 30–50°N for the midlatitudes, and (c) north of 60°N and south of 60°S for the high latitudes.

In the tropics (Figure 8a) there is a pronounced minimum during boreal late summer in the absolute values of the AoA tendency due to the residual circulation T_{rc} and a little bit less pronounced minimum due to the eddy mixing T_{em} (black and gray lines in Figure 8a). The total tendency, $\partial_t\overline{\Gamma}$ (red line), is much

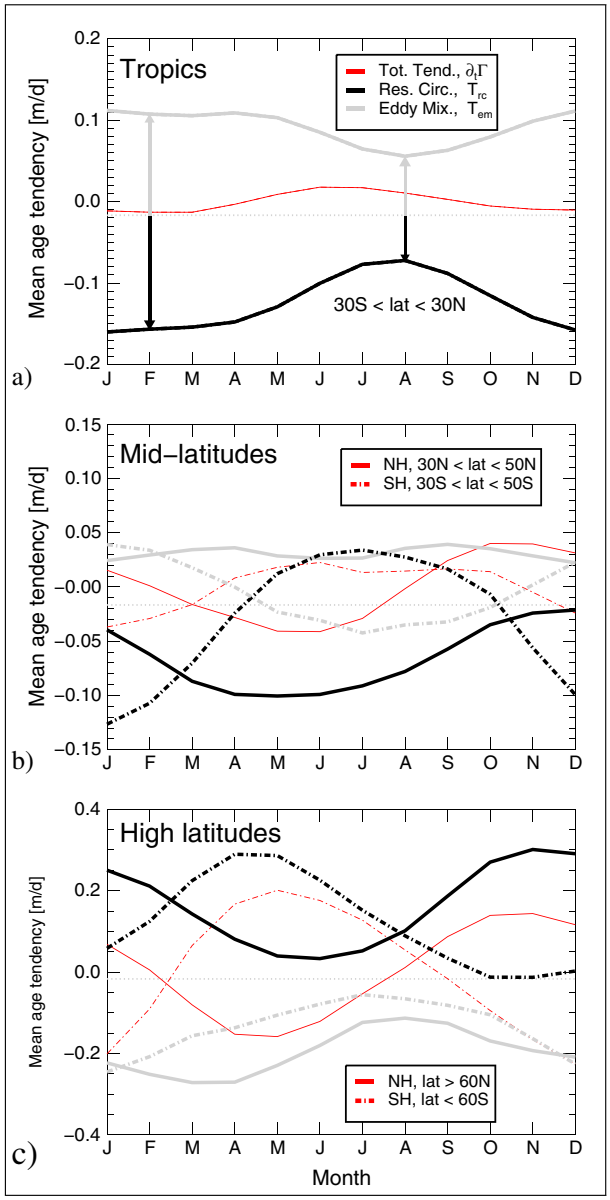

Figure 8. Seasonality of the total tendency of AoA ($\partial_t\overline{\Gamma}$, red) and its decomposition into the mass-weighted contributions of the residual circulation (T_{rc}, black) and of the eddy mixing (T_{em}, gray) for (a) tropics, (b) middle, and (c) high latitudes. The relative importance of both terms can be derived from the relative distance of the black and gray lines to the dashed gray line (arrows, see text for more details). All seasonalities are averaged over the vertical range between $\theta = 380$ and 450 K. The contributions of the NH and SH in Figures 8b and 8c are plotted by using solid and dashed lines, respectively.

smaller if compared with its respective contributions T_{rc} and T_{em}. The residual between $\partial_t\overline{\Gamma}$ and $T_{rc} + T_{em}$ is smaller than 20% if compared with the amplitude of $\partial_t\overline{\Gamma}$ (not shown). Negative and positive values of $\partial_t\overline{\Gamma}$ (i.e., relative to zero line) describe periods when AoA becomes younger (from January to May) and older (from May to December), respectively.

Equation (2) provides even more insights into the undergoing transport processes. To take into account the constant 1 in equation (2), we equally distribute it between the terms T_{rc} and T_{em}. Thus, the absolute value of the term $T_{rc} + 0.5$ is described by the distance between T_{rc} (black) and the line $y = -0.5$ which in here used units (month/day) is given as $y = -1/60$ (dotted gray). Similarly, T_{em}+0.5 is given by the distance between T_{em} (gray) and $y = -1/60$ (dotted gray) because T_{em} is positive.

In particular, the black and gray arrows shown for February and August quantify the relative importance of T_{rc} and T_{em} to the total tendency $\partial_t\overline{\Gamma}$ during these two months. Thus, the oldest air in the TTL can be found in August (see Figure 3, top) because during boreal summer, the contribution of the residual circulation is smaller than the contribution of eddy mixing. Although the absolute values of T_{rc} and T_{em} increase during late winter, the sign of their difference changes leading to youngest air in the TTL around April.

In Figure 8c, the seasonality of $\partial_t\overline{\Gamma}$ is calculated for the high latitudes. Both hemispheres show almost the same seasonality which is shifted in phase by half a year. For example, the strongest decrease of AoA in the NH takes place at almost the same time as the strongest increase of AoA in the SH, i.e., around May.

The residual circulation contributions (T_{rc}) are comparable between the hemispheres if the same seasons are considered (compare black solid to black dashed line shifted by 6 months). Nevertheless, the NH T_{rc} is somewhat larger throughout the year. This difference is a net result of two also small opposite effects: larger descent rates in the NH than in the SH and smaller vertical AoA gradients in the NH than in SH.

However, the clear annual cycles of the NH and SH residual circulation tendencies are contrasted by almost "out of phase" time dependence of the eddy mixing term T_{em} (gray lines). The absolute value of T_{em} in the NH is larger than in the SH throughout the year. The annual means (in month/day) of all terms are as follows: NH, $T_{rc} = 0.16$, $T_{em} = -0.20$; SH, $T_{rc} = 0.11$, $T_{em} = -0.14$, which yield almost vanishing AoA tendencies of

the annual mean (see equation (2) and take the constant 0.03 month/day into account). We conclude that the hemispheric asymmetry of AoA originates from the hemispheric differences in the residual circulation *and* eddy mixing with both contributions larger for the NH than for the SH. Furthermore, the seasonality of these hemispheric differences is different: in the NH T_{em} is always larger during the same season, whereas the absolute value of T_{rc} is always larger during the same time than in the SH.

Finally, Figure 8b shows the decomposition of the AoA tendencies calculated for the midlatitudes between 30 and 50°. First of all, the absolute values are smaller than those in the high latitudes and even in the tropics. Furthermore, the tendencies of the residual circulation and eddy mixing act in the opposite direction if compared with the polar regions in Figure 8c. The residual circulation in the NH tends to make the air younger throughout the year, whereas in the SH between May and October this contribution becomes positive (note a large amplitude of T_{rc} in the SH). Similarly, eddy mixing in the NH tends to enhance the AoA throughout the year whereas T_{em} in the SH is always smaller even with negative tendencies between May and October.

4.3. Relation to the BD Circulation

A large annual cycle in temperature in the TTL is a well-known feature of the general circulation that is primarily associated with the annual cycle of upwelling in the ascending branch of the BD circulation [see, e.g., *Randel et al.*, 2007], although a semiannual cycle would be expected for an aqua-planet as a consequence of the simple fact that the sun crosses the equator twice per year. This pronounced hemispheric asymmetry also manifests in the annual cycle of the AoA shown in Figure 8a. According to our discussion, the annual cycle of the net effect between the residual circulation (stronger in boreal winter-spring) and eddy mixing (stronger in summer-fall) results in respective younger or older mean age in the lower tropical stratosphere.

However, the relation of the high and middle latitudes AoA tendencies analyzed in Figures 8c and 8b to the deep and shallow branches of the BD circulation is more subtle. While in the polar regions, the residual circulation part (T_{rc}) can be assigned to the deep branch of the BD circulation with strongest diabatic descent during fall-winter in each hemisphere (black solid and dashed lines in Figure 8c), the seasonality of the eddy mixing part (T_{em}, gray lines) is almost the same as the seasonality of the EP flux divergence at $\theta = 400$ K describing the forcing of the shallow branch of the BD circulation (Figure 6, bottom). The minimum of the absolute value of T_{em} in the SH coincides well with the SH minimum of the EP flux divergence diagnosed in Figure 6 (bottom). In addition, the maxima of the EP flux divergence in January in the SH and in May in the NH are well represented by the strongest (absolute) contribution of T_{em} in Figure 8c.

Thus, the eddy mixing tendency of the AoA in polar region is well correlated with the enhanced activity of the shallow branch of the BD circulation and tends to decrease AoA in this region throughout the year. In contrast, in midlatitudes, eddy mixing always increases the AoA in the NH as well as between October and May in the SH (Figure 8b). Strong similarities in the seasonality of the T_{rc} and T_{em} terms in Figure 8b with the seasonality of the EP flux divergence at $\theta = 400$ K (Figure 6, bottom) can be diagnosed, e.g., largest negative values of T_{rc} in May and January in the NH correspond well to respective maxima in the EP flux divergence, the absolute maximum of T_{rc} in Juli in the SH is only $\approx$1 month earlier than the pronounced minimum of the EP flux divergence. Thus, we conclude that the shallow branch of the BD circulation is mainly responsible for the seasonality of the AoA tendencies in the midlatitude lower stratosphere.

5. Discussion

An important point is the applicability of our Eulerian-based diagnostic for the understanding of the BD circulation. By using residual circulation trajectories, i.e., trajectories driven by the (time-dependent) residual mean meridional and vertical velocities, *Birner and Bönisch* [2011] presented a Lagrangian view of the deep and shallow branches of the BD circulation. They found a clear time-scale separation between these two branches with much smaller transit times into the midlatitudinal lowermost stratosphere than into the polar latitudes and with a transition region around $\pm 60°$. However, they did not include the effect of eddy mixing that is taken into account in our study albeit from the Eulerian rather than from the Lagrangian perspective.

As recently pointed out by *Garny et al.* [2014], the observed distribution of AoA is an integral process of advection and mixing that from a 2-D Lagrangian perspective is determined both by transport along the

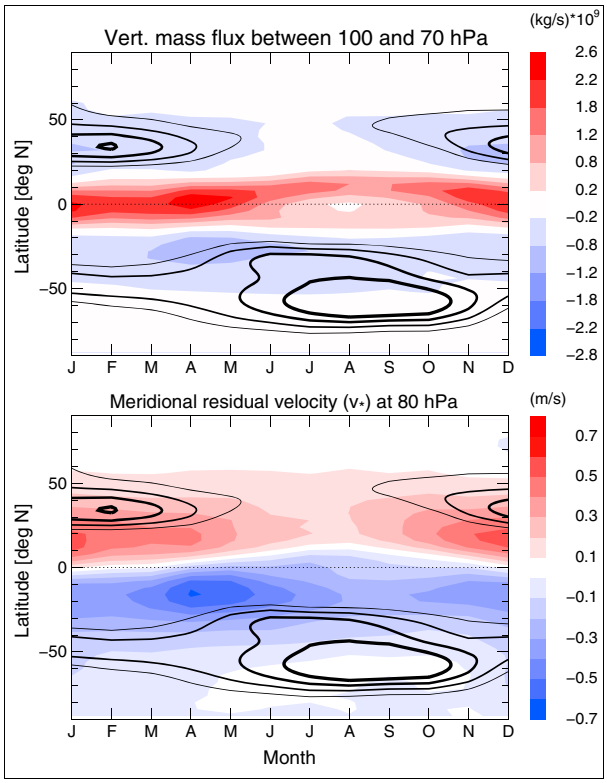

Figure 9. Seasonality of (top) the net vertical mass flux between 100 and 70 hPa and (bottom) the meridional residual velocity $\overline{v}^*$ at 80 hPa. Black lines are the westerlies as in Figure 6 (bottom).

residual circulation and by eddy mixing. Nonlocal processes which have happened along the trajectory in the past may influence AoA at the considered location and time. Thus, a local, Eulerian analysis of time-tendencies and forcing has its limitation [see also *Abalos et al.*, 2013]. In our approach we do not completely solve this problem but give a reasonable interpretation of AoA by averaging the 2-D forcing (Figure 7) over regions (Figure 8) where on a seasonal time scale the contributions of the deep and shallow branches of the BD circulation are almost separated. However, the hemispheric differences of AoA caused by the deep branch of the BD circulation may have longer history for which Lagrangian analysis would be more appropriate.

A common procedure to quantify the strength of the BD circulation is to calculate vertical mass fluxes transported by the different branches of the BD circulation. Using ERA-Interim data as is done here, the seasonal differences in such mass fluxes were recently discussed by *Lin and Fu* [2013]. They found that half of the mass ascending through 100 hPa is transported poleward before reaching 70 hPa and that roughly half of the mass passing 70 hPa ascends through 10 hPa. Using pressure as the vertical coordinate and the TEM vertical velocity $\overline{w}^*$, we get for the annual mean of the upward mass fluxes through 100 and 70 hPa values of 13.8 and 6.9×10^9 kg/s, respectively, which correspond fairly well to the values of 12.8 and 6.2×10^9 kg/s reported in *Lin and Fu* [2013] where a different time period was analyzed (1980–2009). The seasonality of the mass fluxes across 70 hPa and between 100 and 70 hPa agrees with previous estimates [*Rosenlof*, 1995; *Seviour et al.*, 2012; *Lin and Fu*, 2013].

To get more insights into the seasonal pattern of the shallow branch of the BD circulation, we show in Figure 9 (top) the latitudinal dependence of the net vertical mass flux between 100 and 70 hPa. The region of upwelling (red) is well-confined to the tropics between ±15° preferentially to the NH, especially from May to November. The downwelling (blue) extends over a much larger latitude range although confined to the latitudes between ±50°. Remarkable is a negligible downward flux in the NH during boreal summer and early fall probably related to the Asian and American monsoons.

Finally, following equation (1), one expects that the EP flux divergence, the meridional residual velocity $\overline{v}^*$ shown in the bottom panel of Figure 6 (here at 80 hPa), and the time-tendency of the zonal wind ($\partial_t \overline{u}$) balance each other to a good approximation. Because of mass conservation, the net mass flux between 100 and 70 hPa shown in Figure 9 (top) is also coupled to $\overline{v}^*$ (more precisely, this mass flux is equal to the meridional derivative of $\overline{v}^*$).

In the NH, the seasonality of the net mass flux agrees qualitatively with the seasonality of forcing of the shallow branch (Figure 6, bottom). Especially between April and May, the wave forcing slows down the subtropical jet and contributes to maximum net upward mass transport between 100 and 70 hPa. During the same time, the strongest downwelling and the largest (negative) values of $\overline{v}^*$ can be found in the SH which are balanced by enhanced zonal winds rather than by the SH wave forcing that becomes weaker during this time (see Figure 6, bottom). The pronounced minimum of the EP flux divergence between June and October in the SH lower stratosphere is related to the influence of a strong Antarctic vortex that

descends during this time from the middle into the lower stratosphere (Figure 2, bottom) and suppresses the wave breaking [*Gerber*, 2012].

However, due to inaccuracies in the off-line calculations of the terms in equation (1), as well as due to the contribution by data assimilation increments, the momentum budget is not exactly closed. Significant residuals have been found in particular for the SH subtropics during fall which are most likely related to the data assimilation increments. Hence, the lack of a closed momentum budget in this region points to poorly resolved dynamics in ERA-interim there.

6. Conclusions

In contrast to mass, the distribution of AoA in the lower stratosphere is governed not only by the residual circulation but also by eddy mixing. The contribution of the residual circulation to the seasonal variation of AoA is driven by the two branches of the BD circulation, transporting almost the same mass but having different seasonalities.

However, the contribution of eddy mixing to the hemispheric asymmetry of AoA in the lower stratosphere is crucial. Eddy mixing that can be related to the wave breaking driving the shallow branch of the BD circulation is always larger in the NH than in the SH. It has a maximum strength during boreal spring in the NH and during boreal winter in the SH, and a pronounced minimum in the SH between June and October.

Thus, in the polar regions around $\theta = 380$ K, oldest air anywhere can be found in September south of 60°S, whereas the youngest air at all was diagnosed during the same month north of 60°N. During March, i.e., after the Sun has symmetrically changed its position, AoA in the polar NH and SH is almost the same. Following our decomposition of the AoA tendency, this hemispheric asymmetry is not only due to a faster residual circulation in the NH than in the SH but also because the effect of eddy mixing transporting younger air into the high latitudes is significantly larger in the NH than in the SH throughout the year.

The annual cycle of AoA in the TTL is characterized by the youngest air in February and oldest air in August. Following our analysis in isentropic coordinates, this is because during boreal winter the contribution of the residual circulation outweighs that of eddy mixing and vice versa during boreal summer. Note that the absolute values of both, residual circulation and eddy mixing, decrease from winter to summer.

Acknowledgments
The European Centre for Medium-Range Weather Forecasts (ECMWF) provided meteorological analysis for this study (ERA Interim). These data are free, available from the ECMWF WEB page: http://data-portal.ecmwf.int/data/d/interim_daily/. The CLaMS model data may be requested from the corresponding author (p.konopka@fz.juelich.de). Excellent programming support was provided by N. Thomas and F. Schaps. The authors thank G. Stiller for her support with the MIPAS data. Access to this data is described in [*Stiller et al.*, 2012]. Finally, we would like to thank all three reviewers for their insightful and probably very time-consuming comments on the paper, as these comments led us to an improvement of the work.

References

Abalos, M., F. Ploeger, P. Konopka, W. J. Randel, and E. Serrano (2013), Ozone seasonality above the tropical tropopause: Reconciling the Eulerian and Lagrangian perspectives of transport processes, *Atmos. Chem. Phys.*, *13*, 10,787–10,794.

Andrews, A. E., et al. (2001), Mean age of stratospheric air derived from in situ observations of CO_2, CH_4 and N_2O, *J. Geophys. Res.*, *314*, 295–32.

Andrews, D. G., J. R. Holton, and C. B. Leovy (1987), *Middle Atmosphere Dynamics*, Acad. Press, San Diego, Calif.

Austin, J., and F. Li (2006), On the relationship between the strength of the Brower-Dobson circulation and the age of stratospheric air, *Geophy. Res. Lett.*, *33*, 221–225, doi:10.1029/2006GL026867.

Birner, T., and H. Bönisch (2011), Residual circulation trajectories and transit times into the extratropical lowermost stratosphere, *Atmos. Chem. Phys.*, *11*, 817–827, doi:10.5194/acp-11-817-2011.

Birner, T., D. Thompson, and T. Shepherd (2013), Up-gradient eddy fluxes of potential vorticity near the subtropical jet, *Geophys. Res. Lett.*, *40*, 5988–5993, doi:10.1002/2013GL057728.

Bönisch, H., A. Engel, J. Curtius, T. Birner, and P. Hoor (2009), Quantifying transport into the lowermost stratosphere using simultaneous in-situ measurements of SF_6 and CO_2, *Atmos. Chem. Phys.*, *9*, 5905–5919.

Bönisch, H., A. Engel, T. Birner, P. Hoor, D. W. Tarasick, and E. A. Ray (2011), On the structural changes in the Brewer-Dobson circulation after 2000, *Atmos. Chem. Phys.*, *11*, 3937–3948, doi:10.5194/acp-11-3937-2011.

Brewer, A. W. (1949), Evidence for a world circulation provided by the measurements of helium and water vapour distribution in the stratosphere, *Q. J. R. Meteorol. Soc.*, *75*, 351–363.

Butchart, N., et al. (2010), Chemistry-climate model simulations of twenty-first century stratospheric climate and circulation changes, *J. Clim.*, *23*, 5349–5374, doi:10.1175/2010JCLI3404.1.

Charney, J. G., and P. G. Drazin (1961), Propagation of planetary-scale distrubances from the lower into the upper atmosphere, *J. Geophys. Res.*, *66*, 83–109.

Dee, D. P., et al. (2011), The ERA-interim reanalysis: Configuration and performance of the data assimilation system, *Q. J. R. Meteorol. Soc.*, *137*, 553–597, doi:10.1002/qj.828.

Diallo, M., B. Legras, and A. Chedin (2012), Age of stratospheric air in the ERA-Interim, *Atmos. Chem. Phys.*, *12*, 12,133–12,154.

Dobson, G. M. B. (1956), Origin and distribution of polyatomic molecules in the atmosphere, *Proc. R. Soc. London A*, *236*, 187–193.

Fueglistaler, S., A. E. Dessler, T. J. Dunkerton, I. Folkins, Q. Fu, and P. W. Motte (2009a), Tropical tropopause layer, *Rev. Geophys.*, *47*, RG1004, doi:10.1029/2008RG000267.

Fueglistaler, S., B. Legras, A. Beljaars, J.-J. Morcrette, A. Simmons, A. M. Tompkins, and S. Uppapla (2009b), The diabatic heat budget of the upper troposphere and lower/mid stratosphere in ECMWF reanalyses, *Q. J. R. Meteorol. Soc.*, *135*, 21–37, doi:10.1002/qj.361.

Garcia, R. R., and W. J. Randel (2008), Acceleration of Brewer-Dobson circulation due to increase in greenhouse gases, *J. Atmos. Sci.*, *65*, 2731–2739.

Garny, H., T. Birner, H. Bönisch, and F. Bunzel (2014), The effects of mixing on age of air, *J. Geophys. Res. Atmos.*, *119*, 7015–7034, doi:10.1002/2013JD021417.
Gerber, E. P. (2012), Stratospheric versus tropospheric control of the strength and structure of the Brewer-Dobson circulation, *J. Atmos. Sci.*, *69*, 2857–2877.
Gettelman, A., P. Hoor, L. L. Pan, W. J. Randel, M. I. Hegglin, and T. Birner (2011), The extratropical upper troposphere and lower stratosphere, *Rev. Geophys.*, *49*, RG3003, doi:10.1029/2011RG000355.
Hall, T. M., and R. A. Plumb (1994), Age as a diagnostic of stratospheric transport, *J. Geophys. Res.*, *99*(D1), 1059–1070.
Haynes, P., and E. Shuckburgh (2000a), Effective diffusivity as a diagnostic of atmospheric transport: 1. Stratosphere, *J. Geophys. Res.*, *105*, 22,777–22,794.
Haynes, P., and E. Shuckburgh (2000b), Effective diffusivity as a diagnostic of atmospheric transport: 2. Troposphere and lower stratosphere, *J. Geophys. Res.*, *105*, 22,795–22,810.
Haynes, P. H., C. J. Marks, M. E. McIntyre, T. G. Shepherd, and K. P. Shine (1991), On the "downward control" of extratropical diabatic circulations by eddy-induced mean zonal forces, *J. Atmos. Sci.*, *48*, 651–678.
Hegglin, M. I., and T. G. Shepherd (2007), O_3-N_2O correlations from the Atmospheric Chemistry Experiment: Revisiting a diagnostic of transport and chemistry in the stratosphere, *J. Geophys. Res.*, *112*, D19301, doi:10.1029/2006JD008281.
Hegglin, M. I., et al. (2014), Vertical structure of stratospheric water vapour trends derived from merged satellite data, *Nat. Geosci.*, *7*, 768–776, doi:10.1038/NGEO2236.
Holton, J. R., P. Haynes, M. E. McIntyre, A. R. Douglass, R. B. Rood, and L. Pfister (1995), Stratosphere-troposphere exchange, *Rev. Geophys.*, *33*, 403–439.
Konopka, P., et al. (2007), Contribution of mixing to upward transport across the tropical tropopause layer (TTL), *Atmos. Chem. Phys.*, *7*(12), 3285–3308.
Konopka, P., J.-U. Grooß, F. Ploeger, and R. Müller (2009), Annual cycle of horizontal in-mixing into the lower tropical stratosphere, *J. Geophys. Res.*, *114*, D19111, doi:10.1029/2009JD011955.
Konopka, P., J.-U. Grooß, G. Günther, F. Ploeger, R. Pommrich, R. Müller, and N. Livesey (2010), Annual cycle of ozone at and above the tropical tropopause: Observations versus simulations with the Chemical Lagrangian Model of the Stratosphere (CLaMS), *Atmos. Chem. Phys.*, *10*(1), 121–132, doi:10.5194/acp-10-121-2010.
Li, F., D. W. Waugh, A. R. Douglass, P. A. Newman, S. Pawson, R. S. Stolarski, S. E. Strahan, and J. E. Nielsen (2012), Seasonal variations of stratospheric age spectra in the Goddard Earth Observing System Chemistry Climate Model (GEOSCCM), *J. Geophys. Res.*, *117*, D05134, doi:10.1029/2011JD016877.
Lin, P., and Q. Fu (2013), Changes in various branches of the Brewer-Dobson circulation from an ensemble of chemistry climate models, *J. Geophys. Res. Atmos.*, *118*, 73–84, doi:10.1029/2012JD018813.
Mahowald, N. M., R. A. Plumb, P. J. Rasch, J. del Corral, and F. Sassi (2002), Stratospheric transport in a three-dimensional isentropic coordinate model, *J. Geophys. Res.*, *107*(D15), 4254, doi:10.1029/2001JD001313.
McKenna, D. S., P. Konopka, J.-U. Grooß, G. Günther, R. Müller, R. Spang, D. Offermann, and Y. Orsolini (2002), A new Chemical Lagrangian Model of the Stratosphere (CLaMS): 1. Formulation of advection and mixing, *J. Geophys. Res.*, *107*(D16), 4309, doi:10.1029/2000JD000114.
Monge-Sanz, B. M., M. P. Chipperfield, A. J. Simmons, and S. M. Uppala (2007), Mean age of air and transport in a CTM: Comparison of different ECMWF analyses, *Geophys. Res. Lett.*, *34*, L04801, doi:10.1029/2006GL028515.
Ploeger, F., P. Konopka, G. Günther, J.-U. Grooß, and R. Müller (2010), Impact of the vertical velocity scheme on modeling transport across the tropical tropopause layer, *J. Geophys. Res.*, *115*, D03301, doi:10.1029/2009JD012023.
Ploeger, F., G. Günther, P. Konopka, S. Fueglistaler, R. Müller, C. Hoppe, A. Kunz, R. Spang, J.-U. Grooß, and M. Riese (2013), Horizontal water vapor transport in the lower stratosphere from subtropics to high latitudes during boreal summer, *J. Geophys. Res. Atmos.*, *118*, 8111–8127, doi:10.1002/jgrd.50636.
Ploeger, F., M. Riese, F. Haenel, P. Konopka, R. Müller, and G. Stiller (2015), Variability of stratospheric mean age of air and of the local effects of residual circulation and eddy mixing, *J. Geophys. Res. Atmos.*, *120*, 716–733, doi:10.1002/2014JD022468.
Plumb, R. A. (1989), On the seasonal cycle of stratospheric planetary waves, *Pure Appl. Geophys.*, *130*, 233–242.
Plumb, R. A. (1996), A "tropical pipe" model of stratospheric transport, *J. Geophys. Res.*, *101*, 3957–3972.
Plumb, R. A. (2002), Stratospheric transport, *J. Meteorol. Soc. Jpn.*, *80*(4B), 793–809.
Pommrich, R., et al. (2014), Tropical troposhere to stratosphere transport of carbon monoxide and long-lived trace species in the Chemical Lagrangian Model of the Stratosphere (CLaMS), *Geosci. Model Dev.*, *7*, 2895–2916.
Randel, W. J., B. A. Boville, J. C. Gille, P. L. Bailey, S. T. Massie, J. B. Kumer, J. L. Mergenthaler, and A. E. Roche (1994), Simulation of stratospheric N_2O in the NCAR CCM2: Comparison with CLAES data and global budget analyses, *J. Atmos. Sci.*, *51*(20), 2834–2845.
Randel, W. J., R. R. Garcia, and F. Wu (2002), Time-dependent upwelling in the tropical lower stratosphere estimated from the zonal-mean momentum budget, *J. Atmos. Sci.*, *59*, 2141–2152.
Randel, W. J., M. Park, F. Wu, and N. Livesey (2007), A large annual cycle in ozone above the tropical tropopause linked to the Brewer-Dobson circulation, *J. Atmos. Sci.*, *64*, 4479–4488.
Rosenlof, K. H. (1995), Seasonal cycle of the residual mean meridional circulation in the stratosphere, *J. Geophys. Res.*, *100*, 5173–5191.
Schoeberl, M. R., A. R. Douglass, B. Polansky, C. Boone, K. A. Walker, and P. Barnath (2005), Estimation of stratospheric age spectrum from chemical tracers, *J. Geophys. Res.*, *110*, D21303, doi:10.1029/2005JD006125.
Seviour, W. J. M., N. Butchart, and S. C. Hardiman (2012), The Brewer-Dobson circulation inferred form ERA-Interim, *Q. J. R. Meteorol. Soc.*, *138*, 878–888.
SPARC (Ed.) (2010), SPARC report on the evaluation of chemistry-climate models, *SPARC Rep. No. 5, WCRP-132, WMO/TD-No. 1526*. [Avaialble at http://www.atmosp.physics.utoronto.ca/SPARC.]
Stiller, G. P., et al. (2008), Global distribution of mean age of stratospheric air from MIPAS SF_6 measurements, *Atmos. Chem. Phys.*, *8*(3), 677–695.
Stiller, G. P., et al. (2012), Observed temporal evolution of global mean age of stratospheric air for the 2002 to 2010 period, *Atmos. Chem. Phys.*, *12*, 3311–3331.
Vallis, G. K. (2006), *Atmospheric and Oceanic Fluid Dynamics*, Cambridge Univ. Press, Cambridge, U. K.
Waugh, D. W., and T. M. Hall (2002), Age of stratospheric air: Theory, observations, and models, *Rev. Geophys.*, *40*(4), 1010, doi:10.1029/2000RG000101.
Wernli, H., and M. Sprenger (2007), Identification and ERA-15 climatology of potential vorticity streamers and cutoffs near the extratropical tropopause, *J. Atmos. Sci.*, *64*, 1569–1586.